



Proc. 7th European Conference on Antennas and Propagation (EuCAP)

## Investigating multi-antenna RFID systems by means of time-varying scattering parameters

E. Denicke  
D. Härke  
B. Geck

### Suggested Citation:

E. Denicke, D. Härke, and B. Geck. Investigating multi-antenna RFID systems by means of time-varying scattering parameters. In *Proc. 7th European Conference on Antennas and Propagation (EuCAP)*, pages 3314–3318, Apr. 2013.

---

This is an author produced version, the published version is available at <http://ieeexplore.ieee.org/>

©2017 IEEE Personal use of this material is permitted. Permission from IEEE must be obtained for all other uses, in any current or future media, including reprinting/republishing this material for advertising or promotional purposes, creating new collective works, for resale or redistribution to servers or lists, or reuse of any copyrighted component of this work in other works.

# Investigating Multi-Antenna RFID Systems by Means of Time-Varying Scattering Parameters

Eckhard Denicke, Dominic Härke, Bernd Geck  
 Institut für Hochfrequenztechnik und Funksysteme, Leibniz Universität Hannover  
 Appelstr. 9A, 30167 Hannover, Germany  
 Email: denicke@hft.uni-hannover.de

**Abstract**—Recently, the use of multi-antenna techniques in backscatter modulation-based systems, mostly known from the application of RFID, has come into the focus of research due to the increasing demand for higher data rates or the extension of the achievable range or reliability. Thus, this contribution describes a measurement testbed for the investigation of multi-antenna backscatter setups, which is based on a vector network analyzer. In contrast to other publications, the VNA is exploited as a multi-channel vector signal analyzer. By evaluating the time-varying scattering parameters of the system the data transmission on the reverse link can be assessed. Together with a tag emulator incorporating a 4-QAM backscatter modulator, a  $1 \times 1 \times 2$  test system is built (1 reader TX, 1 tag scattering and 2 reader RX-antennas). Measurement results in terms of the symbol error ratio with two signal processing methods in conjunction with maximal ratio combining are presented for various signal-to-noise levels at a center frequency of 5.8 GHz.

**Index Terms**—multi-antenna RFID systems, backscatter modulation, 4-QAM backscatter modulator, time-varying scattering parameters, symbol error ratio measurements

## I. INTRODUCTION

Within the last years the principle of backscatter modulation, mostly known from the application of radio-frequency identification (RFID) [1], is more and more spreading into new fields of application as a passive or semi-passive technology for low-power wireless data exchange. This progress is attended by a demand for higher data rates or the extension of the achievable range or reliability. Since in multipath environments backscatter systems suffer from fading effects, which are more severe than in classical "one way" communication systems [2], multi-antenna techniques in RFID-based systems have come into the focus of research to overcome this drawback in order to enhance the system performance [3]. Multiple antennas can be applied at the reader and at the RFID tag as well.

In general, a backscatter system can be divided in a forward and a reverse link. The forward link is like a common communication link, since the reader is transmitting an inquiry by sending a modulated signal itself. With multiple transmit antennas at the reader and multiple antennas at the tag, the forward link can be described as a classical multiple-input multiple-output (MIMO) link.

On the reverse link information is transmitted from the tag via the reflection of a continuous wave (CW) signal sent from the reader by modulating the tag antenna load corresponding to

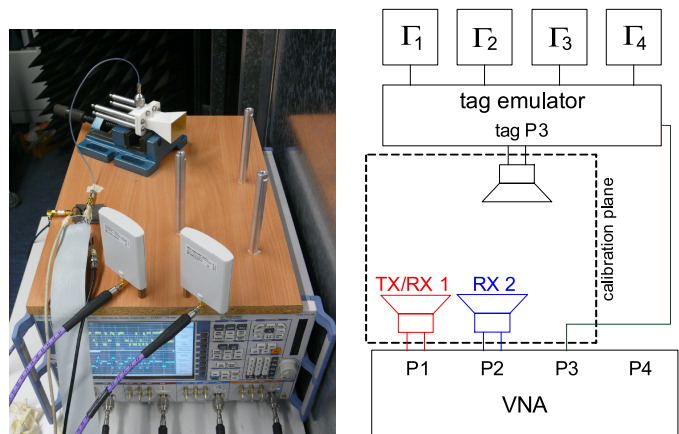


Figure 1. Measurement setup

the data to be transmitted. Consequently, the reverse link with its dyadic channel structure is more interesting to investigate. Thus, this contribution deals with a measurement testbed to investigate the data transmission on the reverse link in order to evaluate the performance of prototype multi-antenna RFID setups, e.g. in terms of the symbol error ratio (SER) in conjunction with multi-antenna signal processing. In Section II the measurement testbed is introduced, followed by a description of the used signal processing in Section III. Measurement results are presented in Section IV before a conclusion is made in Section V.

## II. MEASUREMENT TESTBED

As multi-antenna backscatter systems can be advantageously described with multiport scattering parameters [4], the system proposed herein is based on a vector network analyzer (VNA) (see Section II-A). In contrast to other publications, the VNA is exploited, besides its duty of measuring the channel matrix, as a multi-channel vector signal analyzer: The CW signal radiated from the transmitting (TX) antenna of the reader, i.e. the VNA, is reflected back to the receiving (RX) antennas in a modulated way from the tag scattering antenna, resulting in measurable time-varying scattering parameters or wave quantities, respectively. By postprocessing the measurement data "offline" in MATLAB (Section III), the data transmission on the reverse link can be assessed. Since an experimental tag emulator is used, no inquiry on the forward link is necessary. In this contribution the setup consists of two reader patch

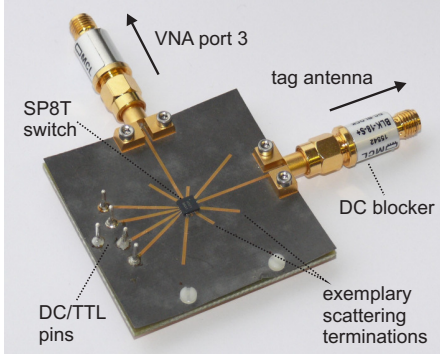


Figure 2. Manufactured 4-QAM modulator

antennas (Huber+Suhner SPA 5600/40/14/0/V), of which one is transmitting at one time and both are receiving, and one tag emulator scattering antenna (pyramidal horn, Seavey Engineering SGA-70L/F), connected to a 4-QAM backscatter modulator (cp. Sec. II-B). This results in a  $1 \times 1 \times 2$  (1 TX/RX) system (cp. notation in [2], whereas "1 TX/RX" has to be added in order to fully identify the system). The system is thus describable with a 3-port scattering matrix, which is terminated by the tag antenna loads resulting in 2-port scattering matrices, which can be measured (cp. [4]). A multiport calibration is conducted as indicated in Fig. 1, whereas port 3 of the VNA is used for comparison channel measurements (direct, no backscatter modulation) (cp. [4]). As an exemplary channel realization a non-line-of-sight multipath scenario with some metallic obstacles is used. Fig. 1 depicts a photo and scheme of the measurement setup.

#### A. Vector Network Analyzer ZVA24

The proposed testbed is based on the VNA Rohde & Schwarz ZVA24 being operated in time-continuous mode. The scattering parameters (reflection and transmission) can be measured over time on all channels synchronously (up to 4 ports) for one excitation. The VNA offers an IF bandwidth of up to 1 MHz and a sampling rate of up to 285.000 samples/s in default factory configuration being sufficient for proof of concept data transmission measurements. It is upgradeable to achieve higher rates. Due to its 4-port configuration with two CW sources, setups of up to  $2 \times L \times 4$  (2 TX/RX) can be realized.

#### B. A 4-QAM Tag Emulator

Besides using multiple scattering antennas [5], modulation schemes of higher order can be used to achieve higher spectral efficiency [6]. Thus, a 4-QAM backscatter modulator was realized, based on a Hittite SP8T microwave switch (HMC321LP4) (cp. Fig. 2). The constellation points (cp. Fig. 4) are achieved with open ended microstrip transmission lines of different lengths at four of the switch output ports and are controlled via TTL with a logic signal output module (Rigol DG-POD-A) in conjunction with a computer for signal processing. Random symbol sequences are used as data to modulate the tag antenna load via the corresponding

switch state. The remaining four switch outputs are used for alternative constellation points (not used for data scattering herein) and for a SMA-port, which offers a direct connection between VNA port 3 and the tag antenna through the switch (cp. Fig. 1), in order to conduct additional measurements for comparison. The VNA is triggered by the logic signal output module at the beginning of each symbol sequence, thus timing or synchronization are not an issue herein.

### III. SIGNAL PROCESSING

In order to coherently combine the backscatter signal from both receiving antennas via maximal ratio combining (MRC) (cp. [7]), the channel influence has to be removed. Since in backscatter-based systems the tag is not able to send a signal by itself and the data transmission is based on measuring the modulated reflection, channel estimation, equalization and symbol detection are different than in classical communication systems.

In general, under the assumption of perfectly matched VNA ports, the measurable reflection scattering parameter, or the four measurable constellation points, respectively, at VNA port 1 can be described in case of a reciprocal channel by ([8],[4]):

$$S_{11_{\text{meas.1,2,3,4}}} = S_{11} + \frac{S_{31}S_{31}\Gamma_{1,2,3,4}}{1 - S_{33}\Gamma_{1,2,3,4}}, \quad (1)$$

whereas the corresponding measurable transmission parameter at VNA port 2 can be modeled by:

$$S_{21_{\text{meas.1,2,3,4}}} = S_{21} + \frac{S_{31}S_{23}\Gamma_{1,2,3,4}}{1 - S_{33}\Gamma_{1,2,3,4}}. \quad (2)$$

The measurable parameters depend on the tag antenna load reflection coefficients  $\Gamma_{1,2,3,4}$  and parameters of the system's 3-port scattering matrix (cp. calibration plane in Fig. 1). The parameters consist of  $S_{11}$ , which is mainly the transmit antenna input reflection and  $S_{21}$  as the direct transmission between antenna 1 and 2 without reflection from the tag. Both parameters account for the static portions, i.e. the DC spectral component, mostly known as the carrier leakage in the measurable scattering parameters and both incorporate static reflections from the far field as well.  $S_{31}$  and  $S_{23}$  account for the transmission between VNA antenna 1 or 2 and the tag antenna (port 3), i.e. for the path loss for instance.  $S_{33}$  describes the tag antenna input reflection as well as accounts for static reflections from the far field (as seen from the tag antenna port 3).

The four tag antenna loads or the respective constellation points  $\Gamma_{1,2,3,4}$  (referring to the systems reference impedance), which have to be detected for data reception, are thus displaced (by  $S_{11}$ ,  $S_{21}$ ) and rotated and scaled (by  $S_{31}S_{31}$ ,  $S_{31}S_{23}$ ) within the complex plane as seen from the VNA ports.

When a binary modulation scheme as on-off keying (OOK) or binary phase shift keying (BPSK) is used, channel estimation and demodulation can e.g. be done based on the trajectory line between both constellation points, which is bisected to get the decision threshold [7]. Since herein a quaternary modulation scheme is used, demodulation is more complex, especially

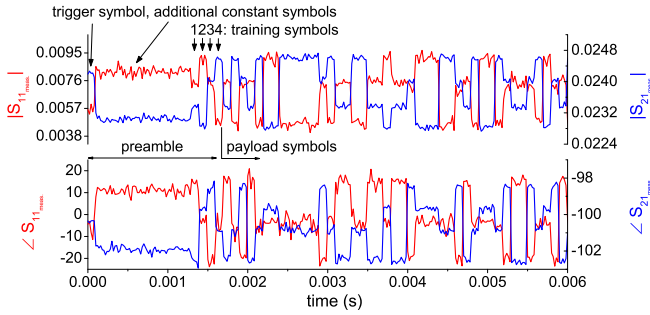


Figure 3. Measured magnitude and phase over time for a random payload symbol sequence with preamble

in case of asymmetrical constellation diagrams, resulting in sophisticated decision regions [9]. Additionally, considering equations 1 and 2, channel effects are more significant, since the term  $\Gamma_{1,2,3,4}/(1 - S_{33}\Gamma_{1,2,3,4})$  leads to a distortion of the relative positions of the constellation points to each other. Since  $S_{33}$  is influenced by the channel scenario, e.g. when other objects are in the near field of the tag antenna, decision rules have to be determined adaptively in dependence of the channel to account for the change of the relative positions of the constellation points.

In this contribution two methods are used for channel estimation and symbol detection.

1) *Method 1*: As described e.g. in [4], if three of the four tag antenna loads are used as known terminations for the system's scattering matrix, all parameters incorporated in equation 1 and 2 can be determined ( $S_{11}, S_{21}, S_{31}S_{31}, S_{31}S_{23}, S_{33}$ ). Thus, in the proposed measurement setup a known training symbol sequence is scattered from the tag before scattering the payload symbols. The channel is assumed to be constant over the data scattering interval.

From the gained scattering parameters of the system's 3-port scattering matrix and the measurable parameters from equation 1 and 2, the original undistorted reference constellation points  $\Gamma_{1,2,3,4}$  can be calculated as follows:

$$\Gamma_{1,2,3,4}^{\text{Ant.1}} = \frac{S_{11\text{meas},1,2,3,4} - S_{11}}{S_{33}S_{11\text{meas},1,2,3,4} + S_{31}S_{31} - S_{11}S_{33}}, \quad (3)$$

$$\Gamma_{1,2,3,4}^{\text{Ant.2}} = \frac{S_{21\text{meas},1,2,3,4} - S_{21}}{S_{33}S_{21\text{meas},1,2,3,4} + S_{31}S_{23} - S_{21}S_{33}}. \quad (4)$$

By this the static signal portions, i.e. the carrier leakage is removed and the relative positions of constellation points are restored. Consequently, the payload symbols can be demodulated by comparing them with the known reference diagram (minimum distance). This method is essentially equivalent to moving the calibration plane of the VNA (cp. equations of the 3-term error model e.g. in [10]), in this case through the channel to the tag antenna port. Since with equation 3 and 4 phase coherency is already achieved, the reconstructed signals from both receiving antennas ( $\Gamma_{1,2,3,4}^{\text{Ant.1}}$  and  $\Gamma_{1,2,3,4}^{\text{Ant.2}}$ ) can then directly be weighted and summed regarding their individual signal-to-noise ratio (SNR) for MRC. Since the narrow band case is assumed, it is sufficient to conduct this equalization procedure only for one frequency point at the center frequency of 5.8 GHz.

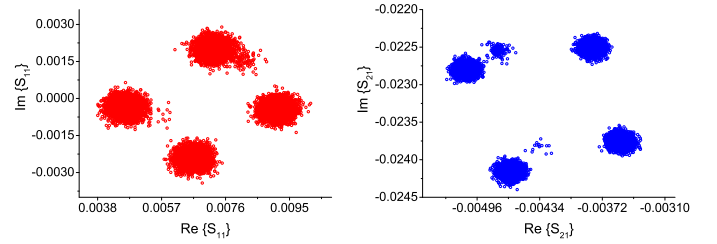


Figure 4. Measured constellation diagrams

2) *Method 2*: This method is more simple. At first, the static (DC) signal portions from the measured scattering parameters  $S_{11\text{meas},1,2,3,4}$  and  $S_{21\text{meas},1,2,3,4}$  are removed. After that, the received constellation points within the known training symbol sequence are taken from the antenna with the highest SNR (herein antenna 2) as the reference symbols for the detection of the following data. The effective channel coefficient for antenna 2 is now essentially unity, whereas the coefficient for antenna 1 with worse SNR is determined to be the averaged ratio of the received training symbol signal values (without DC) and the reference symbols (as derived from the signal at antenna 2). The channel influence for the following symbols at antenna 1 is then removed through division by its channel coefficient. By this the received constellation points of antenna 1 are thus scaled and rotated by the inverse channel coefficient, mapping them to the reference symbols from antenna 2. This is feasible since even the deteriorated constellation diagram positions are the same at both antennas (common term  $\Gamma_{1,2,3,4}/(1 - S_{33}\Gamma_{1,2,3,4})$ ). After that both signals can be combined according to MRC and symbol decision is made.

#### IV. MEASUREMENT RESULTS

For verification of the measurement testbed and the signal processing several backscatter data transmission measurements were conducted with the setup depicted in Fig. 1, which was additionally shielded with absorber to avoid the reception of spurious signals. As data, random sequences with a symbol rate of 10 kHz were used, whereas the sampling rate was set to 50 kHz in conjunction with a VNA IF-bandwidth of 100 kHz. The gained samples are integrated over one symbol interval, which is equivalent to matched filtering with a rectangular pulse shape. Fig. 3 depicts exemplary measured scattering parameters for reception at the VNA antennas 1 and 2 ( $S_{11\text{meas}}$  and  $S_{21\text{meas}}$ ) over time for a scattered random payload symbol sequence (before matched filtering). In addition to the four training symbols within the preamble, two additional symbols, otherwise not used for data transmission, are scattered from the modulator. The first symbol occurs simultaneous to the triggering of the VNA, followed by a constant sequence to identify the beginning of the payload sequence more easily. Fig. 4 depicts the corresponding measured asymmetric constellation diagrams for the total sweep duration of  $\sim 0.3$  s, identifying both the four data symbols and the two additional preamble symbols.

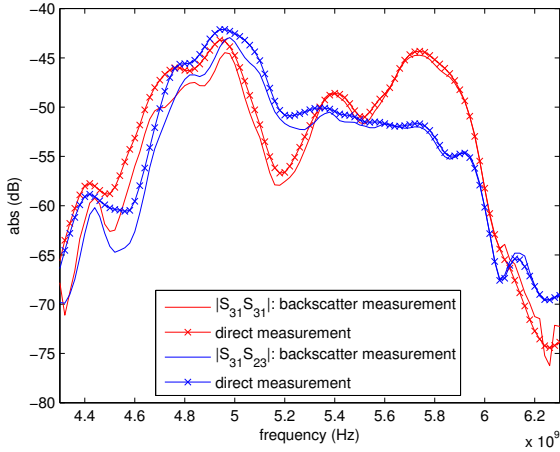


Figure 5. Effective channel transmission  $|S_{31}S_{31}|$  and  $|S_{31}S_{23}|$

The signals from both reader RX-antennas are combined and postprocessed in MATLAB according to the two methods in conjunction with maximal ratio combining (MRC) in order to present SER measurements for various signal-to-noise levels. The different signal-to-noise levels were achieved by varying the transmit power of the VNA. Since the actual noise power of the VNA receivers and thus the SNR is highly dependent on the actual receive power of the VNA ports due to internal adaptive amplification, calibration measurements for the utilized channel scenario were conducted prior to the backscatter data measurements. The noise level at the used IF-bandwidth was determined for the specific transmit power during a static scattering state of the tag emulator by calculating the signal power without DC spectral component, whereas signal plus noise power could be observed during data scattering.

Besides the transmit power, the individual SNR for each receive antenna is on the one hand determined by the effective channel transmission in the selected channel scenario, i.e. the product of the transmission parameters of the forward and the reverse link ( $|S_{31}S_{31}|$  for antenna 1,  $|S_{31}S_{23}|$  for antenna 2). Fig. 5 depicts the magnitude of the effective channel transmission, which can be used to estimate the SNR as well. The curves with crosses are gained via direct measurement with the VNA through the additional tag input port (cp. [4]), whereas the curves without crosses are achieved via backscatter measurement only (*method 1*).

On the other hand the used VNA receiver ports exhibit an inherent noise level difference, leading to a SNR degradation of about 13 dB for port 1. This is due to the fact, that at port 2 a transmitted wave from port 1 is measured, whereas port 1 measures its own reflected wave. Consequently, VNA internal reflections as well as the transmit antenna input reflection limit the measurement accuracy and the dynamic range of port 1, since e.g. a suitable amplification of the weak tag signal is prevented. In the following, the SNR at antenna 2 is set as the reference for comparison.

Fig. 6 depicts the measured constellation diagrams after

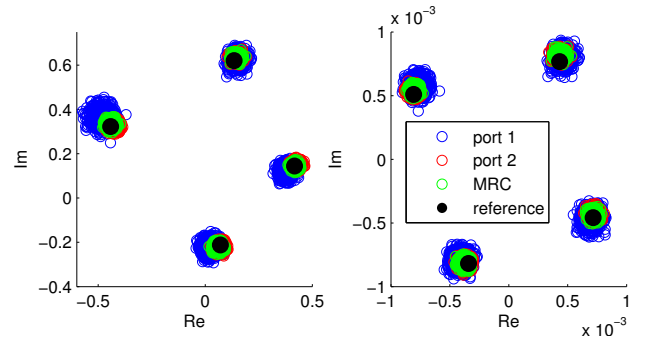


Figure 6. Measured constellation diagrams for port 1 and 2 and for MRC at SNR  $\approx 30$  dB (at reference port 2), after processing with *method 1* (left-hand side) and 2 (right-hand side)

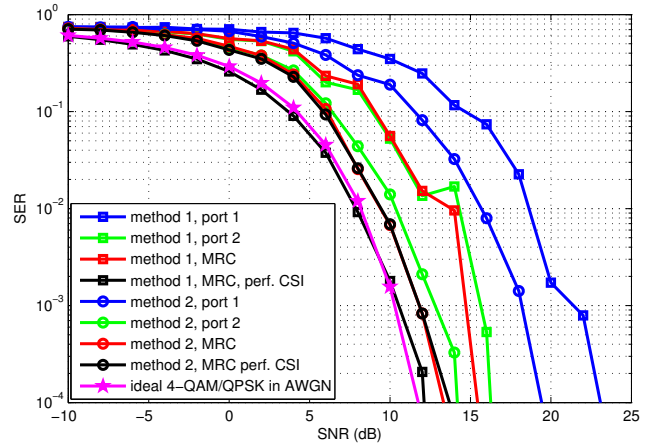


Figure 7. SER over SNR

processing with *method 1* and 2. Although the channel loss for antenna 1 at 5.8 GHz is smaller than for antenna 2 (cp. Fig. 5:  $|S_{31}S_{31}| \approx -45.3$  dB,  $|S_{31}S_{23}| \approx -52.8$  dB), the SNR degradation at port 1 as described above leads a SNR difference of about  $-5.5$  dB for antenna 1 in comparison to antenna 2, so consequently the gain in SNR with MRC is limited. The congruence with the known reference symbols is verified for antenna 2, whereas the congruence for antenna 1 is worse due to the channel estimation at lower SNR.

Fig. 7 depicts the results for the measured SER performance in dependence of the SNR. The SER was averaged over a multitude of measurement sequences. For comparison the theoretical SER results for an ideal 4-QAM/QPSK in a channel with additive white gaussian noise (AWGN) is shown. As stated above, the SNR at antenna 2 is set as the reference for SNR. For both methods the degraded SNR of antenna 1 is obvious, resulting in a shift of the SER curve by about 5.5 dB in comparison to antenna 2. All curves exhibit the slope as expected in an AWGN scenario. In general, *method 2* performs better than *method 1* for channel estimation at the corresponding SNR, whereas for perfect channel state information (perf. CSI) *method 1* outperforms *method 2*. The gain by MRC is visible for *method 1* mainly in case of perfect

CSI, whereas for *method 2* the gain by MRC with and without perfect CSI is almost identical. The ideal channel knowledge is gained from measurements at a high SNR of 30dB. This could be achieved in practice by e.g. scattering longer training sequences to gain more samples for integration.

Future work includes the investigation of the reliability of the methods in different antenna scenarios and the adaption of other types of sophisticated receiver algorithms (cp. [11]).

## V. CONCLUSION

In this contribution a measurement testbed for the investigation of multi-antenna backscatter setups is presented, which is based on a vector network analyzer being exploited as a multi-channel vector signal analyzer. By evaluating the time-varying scattering parameters the data transmission on the reverse link can be assessed. A 4-QAM tag emulator is introduced and SER measurements for a  $1 \times 1 \times 2$  (1 TX/RX) test system at 5.8 GHz for various signal-to-noise levels in conjunction with MRC are presented. Two signal processing methods are proposed, one based on moving the VNA calibration plane to the tag antenna port, the other one on comparison of the data signal to a training sequence.

## REFERENCES

- [1] P. Nikitin and K. Rao, "Antennas and propagation in uhf rfid systems," in *RFID, 2008 IEEE International Conference on*, pp. 277–288.
- [2] J. Griffin and G. Durgin, "Gains for RF tags using multiple antennas," *Antennas and Propagation, IEEE Transactions on*, vol. 56, no. 2, pp. 563–570, feb. 2008.
- [3] N. C. Karmarkar, *Handbook of Smart Antennas for RFID Systems*. John Wiley & Sons Ltd., 2010.
- [4] E. Denicke, M. Henning, H. Rabe, and B. Geck, "The application of multipoint theory for mimo rfid backscatter channel measurements," in *Microwave Conference (EuMC), 42nd European*, 2012.
- [5] M. Ingram, M. Demirkol, and D. Kim, "Transmit diversity and spatial multiplexing for rf links using modulated backscatter," in *Proceedings of the International Symposium on Signals, Systems, and Electronics, Tokyo, JAPAN*, July 24-27 2001.
- [6] S. Thomas, E. Wheeler, J. Teizer, and M. Reynolds, "Quadrature amplitude modulated backscatter in passive and semipassive uhf rfid systems," *Microwave Theory and Techniques, IEEE Transactions on*, vol. 60, no. 4, pp. 1175–1182, april 2012.
- [7] C. Angerer, R. Langwieser, G. Maier, and M. Rupp, "Maximal ratio combining receivers for dual antenna rfid readers," in *Wireless Sensing, Local Positioning, and RFID, 2009. IMWS 2009. IEEE MTT-S International Microwave Workshop on*, 24-25 2009.
- [8] D. Kuester, D. Novotny, J. Guerrieri, R. Dieren, and Z. Popovic, "Reference modulation for calibrated measurements of tag backscatter," in *RFID (RFID), 2011 IEEE International Conference on*, april 2011, pp. 154–161.
- [9] H.-Y. Chen, A. Bhadkamkar, T.-H. Chou, and D. van der Weide, "Vector backscattered signals improve piggyback modulation for sensing with passive uhf rfid tags," *Microwave Theory and Techniques, IEEE Transactions on*, vol. 59, no. 12, pp. 3538–3545, dec. 2011.
- [10] B. Schiek, *«Grundlagen der Hochfrequenz-Messtechnik»*. Springer, Berlin Heidelberg New York, 1999.
- [11] C. Angerer, R. Langwieser, and M. Rupp, "Rfid reader receivers for physical layer collision recovery," *Communications, IEEE Transactions on*, vol. 58, no. 12, pp. 3526–3537, 2010.